Eur. Phys. J. D **12**, 403–413 (2000)

THE EUROPEAN PHYSICAL JOURNAL D

EDP Sciences

Mechanical bistability in an optical lattice

P.M. Visser[a] and G. Grynberg

Laboratoire Kastler-Brossel, Unité de recherche de l'École Normale Supérieure et de l'Université Pierre et Marie Curie[b], 24 rue Lhomond, 75231 Paris Cedex 05, France

Received 23 May 2000 and Received in final form 17 August 2000

Abstract. A probed optical lattice is modelled as a driven anharmonic oscillator with noise. For specific values of the probe intensity and detuning, atoms are forced in bistable solutions. The friction and fluctuations that arise from laser cooling, determine the equilibrium between these two modes of vibration. The distribution determines the absorption spectrum and the transient emission spectrum that is emitted by the optical lattice after the probe has been switched off.

PACS. 32.80.Lg Mechanical effects of light on atoms, molecules, and ions – 42.50.Md Optical transient phenomena: quantum beats, photon echo, free-induction decay, dephasings and revivals, optical nutation, and self-induced transparency – 42.65.Pc Optical bistability, multistability, and switching

1 Introduction

Optical lattices [1–4] are popular systems often used as scale model in classical and quantum mechanics. They are formed when atoms are placed in the periodic light field that results from the superposition of a number of plane optical waves. Laser cooling puts the atoms into a single internal state, where they are subject to the light-shift potential. Although this potential is anharmonic, as shown experimentally [5,6], most situations were analysed and discussed in the harmonic approximation. If an optical lattice is probed by a weak-intensity beam of tunable frequency [7], the atoms undergo a periodic force oscillating at the difference frequency between probe and lattice waves. This turns the system into a driven anharmonic oscillator, where the nonlinearity results from the higher potential regions which were weakly populated in the undriven case. The driven optical lattice may therefore be an interesting physical system to study phenomena like chaos [8], non-linear resonances [3] and mechanical bistability [9].

This paper presents a theoretical study of bistable motion in an optical lattice. Bistability can occur because the resonance frequency of a nonlinear oscillator depends on the amplitude of oscillation [10]. A well-know microscopic demonstration of mechanical bistability is formed by electromagnetically driven electrons revolving in a static magnetic field [11,12]. In this system dissipation is weak and a very accurate measurement of the hystereses in the resonance spectrum can be made. Atoms in an optical lattice, however, are also subject to friction forces and diffusion resulting from spontaneously emitted photons [13]. Bistability is affected by these fluctuations. One can imagine that the atom jumps continuously between the different stable solutions. The population of the stable states is determined by the dissipative forces. This stands in contrast to the electron cyclotron (and to most optically bistable devices [14]), where only one stable state is excited at a time.

The system of a driven anharmonic oscillator in contact with a thermal bath has been studied both as a classical and as a quantum mechanical system. Numerical solutions of the master equation [15,16] and of the stochastic Schrödinger equation [17] provide insight into the quantum-classical correspondence. We present a classical analysis of the driven anharmonic oscillator, as a model of a driven optical lattice. The equations of motion are studied in the frame rotating at the frequency of the driving force. In the rotating-wave approximation, the time evolution of the phase-space distribution is described by a Fokker-Planck equation with a Hamiltonian that is time independent in the rotating coordinates. This approximation is appropriate in the parameter range where chaos does not occur (or possibly swamped in the noise). In this case, the Fokker-Planck equation has an equilibrium solution. As an application of the model to an optical lattice, we use this solution to calculate the probe absorption spectrum and the transient emission by the lattice after the switch-off of the probe beam (Sects. 6 and 7). Our method can be generalized in a number of directions. A more realistic description, with several internal states could be used to properly account for the laser cooling. The Fokker-Planck equation could also be extended to a Wigner-function approach to include quantum-mechanical coherences and fluctuations. As we have recently shown [9], however, the basic ingredients to account for the observed phenomena are already present in this limited model.

[a] e-mail: `paul.visser@lkb.ens.fr`
[b] laboratoire associé au CNRS (UMR 8552)

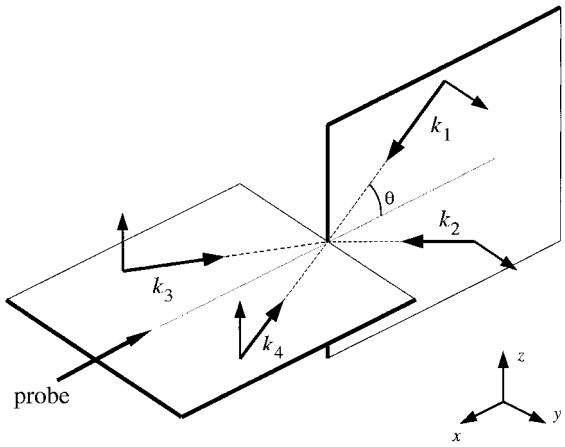

Fig. 1. The scheme of the standard lin ⊥ lin configuration with four laser beams is a possible setup to which our model can be applied. The probe beam is directed along the x-axis of symmetry. The interference of the lattice and probe beams generates the optical potential given in equation (1).

2 Optical lattice as anharmonic oscillator with noise

Although we will limit the analysis to one dimension, the starting point of the physical problem is a three-dimensional four-beam optical lattice [18], which results from the superposition of monochromatic waves with frequency ck and wave vectors directed under an angle θ with respect to the symmetry axis. A possible configuration is the standard lin ⊥ lin setup as illustrated in Figure 1. Light forces arrange the atoms in a periodic structure with a spatial frequency along Ox $2\kappa = 2k\cos\theta$. This system is now probed with a weak-intensity beam of tunable frequency. We take this wave in the x-direction, and call δ the difference frequency from the carrier waves. In the following, we restrict the study of the atomic dynamics to the x-axis only. This one-dimensional approach is reasonable when the natural eigenfrequencies found for the transverse motion differ from those found along Ox (see Fig. 1). We further assume that the optical detuning of the light waves from the atomic transition is much larger than the natural line width, so that dissipative forces (radiation pressure) can be neglected compared to the reactive forces [19]. Furthermore, we assume that a single optical potential is sufficient to describe the anharmonic motion of the atoms. This potential can either be the dipole potential of a far-off resonant lattice [20–22], the effective potential in the jumping regime [13,23] or the lower potential curve of the oscillating regime [24,25]. We thus suppose that the force acting on the atom is the gradient of the potential

$$V(x,t) = -\frac{1}{2}V_\mathrm{l}\cos 2\kappa x + V_\mathrm{p}\epsilon_+ \sin(kx+\kappa x-\delta t) + V_\mathrm{p}\epsilon_- \sin(kx-\kappa x-\delta t). \quad (1)$$

The first term $V(x) = -\frac{1}{2}V_\mathrm{l}\cos 2\kappa x$ is the potential of the lattice without probe, with height V_l proportional to light intensity I_l. The two time-dependent components in equation (1) arise from the interference between the probe beam and the lattice waves, and therefore has strength $V_\mathrm{p} = V_\mathrm{l}\sqrt{I_\mathrm{p}/I_\mathrm{l}}$ when the probe beam intensity is I_p. They have numerical prefactors ϵ_+ and ϵ_- on the order of unity which depend on the specific atomic transition and on the beam polarization.

The mechanics of the atoms in the lattice is described by Newton's equations

$$\dot{p} + \gamma p + \frac{\mathrm{d}}{\mathrm{d}x}V(x,t) = F(t), \quad m\dot{x} = p, \quad (2)$$

with the potential (1). In our model, the friction has damping rate γ and the Langevin force $F(t)$ has zero mean and is delta correlated:

$$\langle F(t)\rangle = 0, \quad \langle F(t')F(t)\rangle = 2R\delta(t'-t).$$

The brackets denote the ensemble average and R is the momentum diffusion constant. The friction and fluctuating forces are modelling the laser cooling due to the coupling to the other potentials [26]. These forces can be assumed to act locally in the jumping regime, where many optical pumping cycles occur during one period of oscillation in the potential well. We do not take into account a position or velocity dependence of γ and R. In absence of the probe beam, $I_\mathrm{p} = 0$ and motion is restricted to the minima located at positions $a_j = j\pi/\kappa$. There the potential is harmonic with vibrational frequency $\omega_0 = \kappa\sqrt{2V_\mathrm{l}/m}$. For low diffusion, the system becomes the damped harmonic oscillator, which has mean fluctuations related to the temperature T by

$$\frac{1}{2m}\langle p^2\rangle = \frac{m}{2}\omega_0^2\langle(x-a_j)^2\rangle = \frac{k_\mathrm{B}T}{2} = \frac{R}{2m\gamma}\cdot \quad (3)$$

The full equation of motion (2) can exhibit a large variety of physical behaviour [27–29]. For the deterministic case, when $R = 0$, there exist regions in parameter space where motion is chaotic, and regions where the system is damped into resonant periodic orbits or higher harmonics and even subharmonics of the driving frequency δ [28–30]. The trajectories can also travel many wavelengths. When position-dependence in the (weak) time-dependent force and higher order non-linear terms in the light-shift force are neglected, the system is equivalent to a thermal Duffin oscillator. In the present study we will only consider motion in a single well, *i.e.* $-\pi < 2\kappa x < \pi$. We also restrict our analysis to periodic states with frequency δ. We will however use the full cosine form (1) and, of course, include noise. Clearly, the model presented here as intended to describe a probed optical lattice, might be applicable to Brownian motion in other driven nonlinear systems.

3 Equations of motion in the rotating frame

In order to study bistability, it will be convenient to use coordinates in the co-rotating frame. We introduce two pairs of variables, the Cartesian co-rotating variables

$u(t), v(t)$ and the corresponding canonical circular coordinates $n(t), \phi(t)$:

$$u + \mathrm{i}v = \sqrt{2n}\,\mathrm{e}^{\mathrm{i}\phi} = (x + \mathrm{i}p/m\delta)\mathrm{e}^{\mathrm{i}\delta t}, \tag{4}$$

for an atom near $a_j = 0$. A pair of first order equations for u, v or n, ϕ is obtained when these relations are substituted in the equation of motion (2). Since the transformation is canonical, the coherent part of this equation derives from the transformed Hamiltonian. It follows directly from the application of the Jacobi theorem [10] that the new Hamiltonian $H(u, v, t)$ is the difference between the Hamiltonian of an harmonic oscillator of stiffness δ and the original Hamiltonian $E(x, p, t)$

$$\begin{aligned} m\delta H(u, v, t) &= \frac{1}{2m}p^2 + \frac{m}{2}\delta^2 x^2 - E(x, p, t) \\ &= \frac{m}{2}\delta^2 x^2 - V(x, t), \end{aligned} \tag{5}$$

where x, p must be expressed in u, v. In the new frame, we make the rotating-wave approximation, which eliminates the time dependence of the driving force. This approximation is fairly good when δ is in the vicinity of ω_0. In the following, nearly resonant excitation is assumed to be dominant compared to other excitation processes, such as parametric or nonlinear resonances. By neglecting all fast oscillating terms in $\mathrm{e}^{\mathrm{i}\delta t}$ the equations of motion become of the form

$$\dot{u} = \frac{\mathrm{d}H}{\mathrm{d}v} - \frac{\gamma u}{2} + \xi, \quad \dot{v} = -\frac{\mathrm{d}H}{\mathrm{d}u} - \frac{\gamma v}{2} + \xi', \quad \text{and} \tag{6}$$

$$\dot{n} = \frac{\mathrm{d}H}{\mathrm{d}\phi} - \gamma n + 2D + \sqrt{2n}\,\xi, \quad \dot{\phi} = -\frac{\mathrm{d}H}{\mathrm{d}n} + \frac{1}{\sqrt{2n}}\xi', \tag{7}$$

for the Cartesian, and for the and circular co-rotating coordinates. In these equations, ξ, ξ' are white noise sources:

$$\langle \xi(t')\xi(t)\rangle = \langle \xi'(t')\xi'(t)\rangle = 2D\delta(t' - t), \quad \langle \xi'(t')\xi(t)\rangle = 0,$$

and the spatial diffusion constant is $D = R/2(m\delta)^2$. The effective Hamiltonian is calculated after substitution of equation (1) in equation (5) and has the form

$$\begin{aligned} H(u, v) = H(n, \phi) &= \overline{H(u, v, t)} \\ &= \frac{1}{2\delta}\Big[\delta^2 n - U(n) - 2f(n)u\Big]. \end{aligned} \tag{8}$$

It is valid for both pairs of equations (6, 7). The overline denotes the time average over one period. The average potential energy of the bare lattice contributes the term

$$U(n) = \frac{2}{m}\overline{V(x)} = -\frac{\omega_0^2}{2\kappa^2}J_0(\kappa\sqrt{8n})$$

to this effective Hamiltonian. Here J_0 is a Bessel function. The probe beam results in a force independent of time with acceleration f given by

$$f(n) = \frac{\omega_0^2}{\kappa^2}\sqrt{\frac{I_\mathrm{p}}{2nI_\mathrm{l}}}\Big[\epsilon_+ J_1((k+\kappa)\sqrt{2n}) + \epsilon_- J_1((k-\kappa)\sqrt{2n})\Big].$$

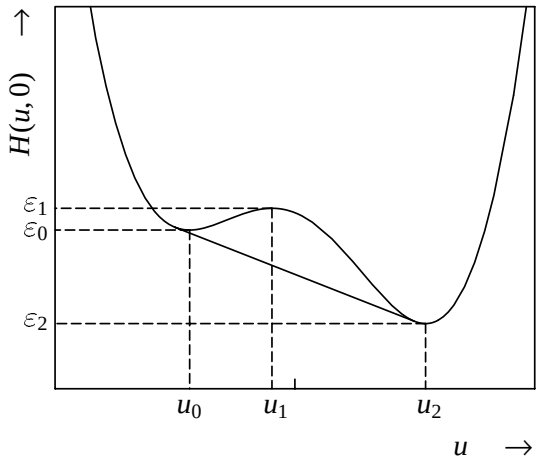

Fig. 2. Projection of the Hamiltonian on the plane $v = 0$. The maximum and minimum, $(u_1, 0)$ and $(u_2, 0)$ and the saddle point $(u_0, 0)$ are indicated. The parameters of force and detuning are $\kappa f = 0.02\omega_0^2$ and $\delta = 0.85\omega_0$.

Since $I_\mathrm{p} \ll I_\mathrm{l}$, higher order terms of the Bessel function J_1 may be neglected and f can be taken as a constant, when the atoms remain reasonably close to the potential minimum. This corresponds to a pure oscillating driving force $mf\cos\delta t$ in the original equation of motion (2). The Hamiltonian $H(u, v)$ has the shape of a sombrero (Mexican hat) when plotted as a function of u, v (see Fig. 2). For nonzero f this hat is tilted in the u-direction. A Hamiltonian of similar form was used in reference [15].

In the rotating-wave approximation, the friction causes damping of the amplitude n, but has no effect on the phase. The momentum fluctuations gives rise to an isotropic diffusion in phase space with the diffusion constant D. The two noise sources of u and v are white and independent. The noise in n and ϕ is also described by two independent noise terms. (They are in fact the linear combinations of the u, v noise, but we use the same notation for simplicity.) Since the corresponding jump factors of the noise in equation (7) are not constant, the stochastic differential equations must have a well defined interpretation rule. In the present paper, we use the Ito interpretation, which assumes that the strength of the noise jumps in n are determined by the value of n just before a jump [31, 32]. This gives rise to a drift term $2D$ caused by the fluctuations. In circular coordinates, such a drift term is expected, since the diffusion must increase the average value of n at $n = 0$, while the noise in n vanishes at the origin.

When $f = 0$, $\gamma = \kappa^2 D = 0$, equation (7) has constant solutions, *i.e.* with $(\dot{n}, \dot{\phi}) = (0, 0)$, for any value of the amplitude and phase when δ is chosen to be equal to the characteristic frequency ω, defined by

$$\omega^2(n) = \frac{\mathrm{d}}{\mathrm{d}n}U = \frac{1}{mn}x\overline{\frac{\mathrm{d}}{\mathrm{d}x}V} = \frac{\omega_0^2}{\kappa\sqrt{2n}}J_1(\kappa\sqrt{8n}). \tag{9}$$

Hence, $\omega(n)$ is the frequency of the free motion in the anharmonic potential well as a function of amplitude. For the rotating-wave approximation to be valid, the rate $\dot{\phi}$ must be small compared to δ. This implies that the motion

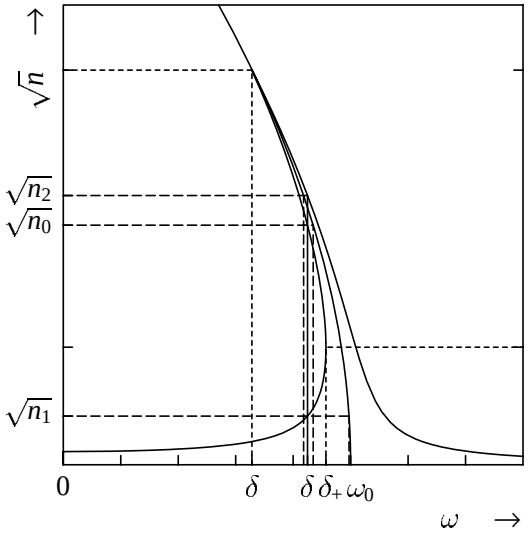

Fig. 3. Resonance curve of an anharmonic oscillator driven with force $\kappa f = 0.02\omega_0^2$ and damped with rate $\gamma = 0.051\omega_0$. The thin solid line represents the free vibrational frequency $\omega(n)$, in absence of driving and damping. Amplitude $\sqrt{n}$ is plotted *versus* frequency ω. In this example the detuning $\delta = 0.85\omega_0$ lies in the range $\delta_- < \delta < \delta_+$, and three stationary solutions can be found. Two high amplitude solutions have vibrational frequencies close to δ and the low amplitude solution almost has the harmonic frequency ω_0, when undriven. The figure shows how these free vibrational frequencies can be determined graphically.

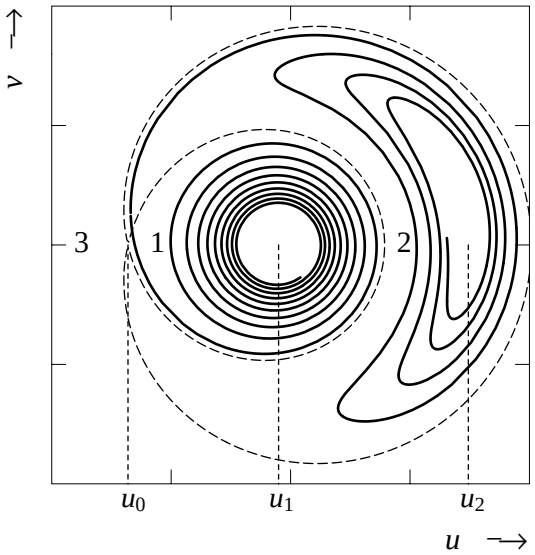

Fig. 4. Trajectories in phase space. The two trajectories that are plotted solid include friction with the damping rate $\gamma = 0.02\omega_0$. These run from the instable point to the stable solutions. The dotted line represent the critical orbit in absence of friction. This divides the phase space in the domains 1, 2 and 3. Force and detuning are $\kappa f = 0.02\omega_0^2$ and $\delta = 0.7\omega_0$.

is approximately harmonic. The non-linear dependence of the vibrational frequency on the amplitude is shown in Figure 3.

4 Bistability without fluctuations

4.1 Stationary solutions

In absence of diffusion, when $D = 0$, the evolution is deterministic and the equations of motion (7), with equations (8, 9) become

$$\delta\dot{n} = fv - \gamma\delta n, \quad 2\delta n\dot{\phi} = (\omega^2 - \delta^2)n + fu.$$

In this situation, fixed stationary solutions with $(\dot{n}, \dot{\phi}) = (0, 0)$ can occur. It follows from elimination of the phase ϕ, using equation (4), that at such a point

$$\gamma^2\delta^2 + (\omega^2 - \delta^2)^2 = 2f^2/n.$$

The driving frequency δ of the stationary solutions is therefore expressed as a function of n by

$$\delta^2(n) = \omega^2 \pm \sqrt{2f^2/n - \omega^2\gamma^2 + \gamma^4/4} - \gamma^2/2. \qquad (10)$$

The two signs correspond to a detuning above and below the resonance frequency $\omega(n)$. When the two branches are connected, a resonance curve with n as a function of δ is obtained, as plotted in Figure 3. It has the shape of a deformed Lorentzian curve and bends over [10]. If the potential is wider than the harmonic potential for large x, the oscillation frequency $\omega(n)$ decreases with n, and the peak turns to the left. For a narrower potential the peak turns to the right. The maximum amplitude is reached at the point where the two branches connect.

We consider the cosine potential which is wider than a harmonic potential. In an interval $\delta_- < \delta < \delta_+$ for the driving frequency, with $\delta_+ < \omega_0$, bistability occurs. Here exist three stationary solutions, instead of one. These we denote by (n_1, ϕ_1), (n_0, ϕ_0), (n_2, ϕ_2), with $n_1 < n_0 < n_2$. The solution 1 is stable and has a small amplitude n_1. One of the two high-amplitude solutions, 2 is also stable but the third solution, labelled with index 0 is instable. The driving frequency is below the resonant frequency $\omega_1 = \omega(n_1)$ of the small-amplitude mode, and slightly above the resonant frequency $\omega_2 = \omega(n_2)$ of the high-amplitude mode, so that $\omega_2 \lesssim \delta \lesssim \omega(n_0) < \omega_1 \lesssim \omega_0$. As shown in Section 6, an atom will start to oscillate with the free vibrational frequency if the driving field is suddenly switched off.

Which of the two stable solutions is excited depends on the initial conditions. Two trajectories that start at the instable point are plotted in Figure 4. At the stable endpoints (n_1, ϕ_1) and (n_2, ϕ_2), position and mechanical energy in the original frame, of course do still oscillate according to

$$\begin{aligned} x(t) &= \sqrt{2n_i}\cos(\phi_i + \delta t), \\ E(x,p) &= \frac{1}{2m}p^2 + V(x) \\ &= \frac{m}{2}\Big[\delta^2 n_i + U(n_i) + fu_i\cos 2(\phi_i + \delta t)\Big]. \end{aligned}$$

The bistability interval is bounded by the points δ_- and δ_+ on the negative branch, where $n_2 = n_0$ and $n_1 = n_0$. These values are determined by equation (10) and $\mathrm{d}\delta/\mathrm{d}n = 0$. The driving force and the amplitudes at these boundaries are found to be related by

$$f^2(n) = \Big(K \pm \sqrt{K^2 + 2\gamma^2\kappa^2 U + \gamma^4/4} + \gamma^2/2\Big) nK, \quad \text{with}$$
$$K(n) = -n\frac{\mathrm{d}}{\mathrm{d}n}\omega^2 = \omega^2 + 2\kappa^2 U = \omega_0^2 J_2(\kappa\sqrt{8n}).$$

This expression of the force can be used in a parameterized plot of the two solutions of $\delta(n)$ *versus* $f(n)$ where the amplitude n is the parameter. The bistability interval can then be read off directly from the resulting figure.

4.2 Hamiltonian motion

In absence of all dissipative forces, *i.e.* when both $D = 0$ and $\gamma = 0$, the trajectories are periodic and have a well defined pseudo energy $\varepsilon = H(n(t), \phi(t))$. Recall that the Hamiltonian surface has the shape of a sombrero. The trajectories in phase space are (horizontal) cross-sections of this surface. The circular valley around the top of the hat is approximately the ring $\omega(n) = \delta$. Since the hat is tilted, the valley has a saddle point and a minimum on opposite sides (see Fig. 2). Of course, the stationary points correspond precisely to the saddle point, the maximum and the minimum. The energy values are denoted with ε_0, ε_1, ε_2. The saddle point at energy ε_0 is the instable point. In the range, $\varepsilon_0 \le \varepsilon \le \varepsilon_1$, the energy is double valued. For these values, one large orbit encloses a second, smaller orbit. In this range, we label the inner orbits with 1 and the outer orbits with 3. The orbits with energies $\varepsilon_2 \le \varepsilon < \varepsilon_0$ have the label 2. Orbits with energy $\varepsilon_1 < \varepsilon$ also have label 3, since they connect to the outer orbits at ε_1. The orbits are thus denoted with $n_i(\varepsilon, t)$, $\phi_i(\varepsilon, t)$ and have periods $T_i(\varepsilon)$, according to their energy ε and phase-space domain $i = 1, 2, 3$. For the stable points we have $n_1(\varepsilon_1, t) = n_1$ and $n_2(\varepsilon_2, t) = n_2$, with phases $\phi_2 = 0$, $\phi_1 = \phi_0 = \pi$. The critical orbit with energy ε_0 crosses the instable point and forms the border between domains 1, 2 and 2, 3 (see Fig. 4). When friction is included, the stable points do no longer coincide with the maximum and minimum of the Hamiltonian, but are slightly displaced. The dynamics in the vicinity of these stable points is described in Appendix A.

5 Bistability under action of fluctuations

5.1 The Fokker-Planck equation

In presence of the diffusion terms, the equations of motion (7) are stochastic, and do not have a stationary state. It is useful to introduce the time-dependent distribution $P(n, \phi, t) = \langle \delta(n - n(t))\delta(\phi - \phi(t))\rangle$ in phase space, defined for the ensemble average of the trajectories. The time-evolution of P is described by the Fokker-Planck equation [32]

$$\dot{P} = \frac{\mathrm{d}}{\mathrm{d}n}\Big[\gamma n - \frac{\mathrm{d}H}{\mathrm{d}\phi} + 2Dn\frac{\mathrm{d}}{\mathrm{d}n}\Big]P + \frac{\mathrm{d}}{\mathrm{d}\phi}\Big[\frac{\mathrm{d}H}{\mathrm{d}n} + \frac{D}{2n}\frac{\mathrm{d}}{\mathrm{d}\phi}\Big]P.$$

This equation is equivalent to the stochastic differential equations (7) for (n, ϕ). One can also verify this particular form most easily by first deriving the Fokker-Plank equation from the stochastic differential equations (6) for the variables (u, v), and then transforming to circular coordinates.

The distribution $P(n, \phi, t)$ does evolve into an equilibrium state. This steady-state solution $P(n, \phi)$ contains the information which determines the absorption rate and the frequency spectrum of scattered light as we shall demonstrate in Sections 6 and 7. Because the Hamiltonian represents a pseudo energy and not the systems free energy, the equilibrium solution is not given by a straightforward Boltzmann solution [31].

5.2 The low-temperature approximation

In the limit of weak diffusion, when D is small, the Fokker-Plank equation can be linearized around a stable point. The steady-state solution of this linearized equation is valid in the vicinity of the stable point. The two local stationary solutions are

$$P_i(n, \phi) = \frac{\alpha_i \gamma}{DC_i T_i(\varepsilon_i)} \exp - \left[\frac{\gamma}{DC_i}\Big|H_i(n, \phi) - \varepsilon_i\Big|\right], \tag{11}$$

for (n, ϕ) near (n_i, ϕ_i), with the effective Hamiltonian H_i and orbit times T_i given in Appendix A, and with

$$C_i = \frac{1}{\delta}\Big[\delta^2 - \omega_0^2 J_0(\kappa\sqrt{8n_i})\Big]. \tag{12}$$

For small friction the original Hamiltonian, equation (8) can be substituted. The absolute value in equation (11) ensures that for both solutions P_1 and P_2 population is maximal at the stable point (n_i, ϕ_i).

Obviously, the full solution in the limit of weak fluctuations is of the form $P(n, \phi) = P_1(n, \phi) + P_2(n, \phi)$. The average width of the two peaks in P are both approximately equal to $2D/\gamma = k_\mathrm{B}T/m\delta^2$, although the peaks can be squeezed as an effect of the Hamiltonian. The average spread in momentum of each of the peaks in the driven case and the momentum width of the undriven system as given in equation (3) are equal. Due to the rotating-wave approximation, however, the width in position is broadened, as compared to the undriven situation. This is understandable, but not quite correct, because for a linear oscillator the spread in position is unaffected by the driving field. On the other hand, the nonlinear potential and driving force actually might very well result in a broadening of the position. The respective populations of the peaks are α_1 and α_2, so that $\alpha_1 + \alpha_2 = 1$. The remaining part of this section is aimed to determine these populations.

5.3 Equilibrium distribution in the low-friction approximation

In order to obtain an analytical expression of the steady-state distribution $P(n,\phi)$, we make the secular approximation. This is valid in the regime of weak relaxation, where both the rates γ and $\kappa^2 D$ are small compared to the orbital frequencies. If we consider the orbital frequency of the high amplitude state, this condition implies $\gamma^2 \ll (\delta-\omega_2)\omega_0$ which can be easily fulfilled experimentally. Of course, in this approximation, the temperature as defined in equation (3) can still have any value. The details of the calculation are presented in the Appendix B. The method consists in deriving a Fokker-Planck equation for the pseudo-energy distribution $F_i(\varepsilon,t)=\langle\delta(\varepsilon-\varepsilon(t))\rangle$, where the index i stands for the domain $i=1,2,3$ in phase space. The equilibrium solution has the form of a Boltzmann distribution

$$\begin{aligned} F_1(\varepsilon) &= \frac{\gamma}{2ND}\exp\frac{\gamma}{DC_1}(\varepsilon-\varepsilon_0),\\ F_2(\varepsilon) &= \frac{\gamma}{ND}\exp\frac{\gamma}{DC_2}(\varepsilon_0-\varepsilon),\\ F_3(\varepsilon) &= \frac{1}{2}F_2(\varepsilon). \end{aligned} \tag{13}$$

Note however that the sign of the exponent changes at the instable point. In these equations, N is a normalization factor. The population of the different domains

$$\alpha_1=\int_{\varepsilon_0}^{\varepsilon_1}\mathrm{d}\varepsilon\,F_1,\quad \alpha_2=\int_{\varepsilon_2}^{\varepsilon_0}\mathrm{d}\varepsilon\,F_2,\quad \alpha_3=\int_{\varepsilon_0}^{\infty}\mathrm{d}\varepsilon\,F_3,$$

are given by

$$\begin{aligned} \alpha_1 &= \frac{C_1}{2N}\Big[\exp\frac{\gamma}{DC_1}(\varepsilon_1-\varepsilon_0)-1\Big],\\ \alpha_2 &= \frac{C_2}{N}\Big[\exp\frac{\gamma}{DC_2}(\varepsilon_0-\varepsilon_2)-1\Big],\\ \alpha_3 &= \frac{C_2}{2N}\cdot \end{aligned} \tag{14}$$

The normalization $\alpha_1+\alpha_2+\alpha_3=1$ therefore determines the value of N. The probability distribution in phase space P at is related to F_i and the Hamiltonian by

$$P(n,\phi,t)=\frac{F_i(H(n,\phi),t)}{T_i(H(n,\phi))}\cdot \tag{15}$$

Here T_i is the period of an orbit of energy ε given by the following integral (where the integration interval ranges from the minimum to the maximum value of n on the orbit):

$$T_i(\varepsilon)=\int\mathrm{d}n\,\frac{4\delta}{\sqrt{8f^2n-(2\delta\varepsilon+U-\delta^2 n)^2}}\cdot \tag{16}$$

The relationship (15) is valid for all times t, not just in the steady state. Near the critical orbit, the period diverges, as described by equation (A.3). Therefore, at the borders of the phase-space regions, the density P drops to zero. This divides the distribution in three separate components corresponding to the three domains in phase space. Two components have peaks at the location of the stable points. The third outer domain only becomes populated at high temperatures. An example of the equilibrium phase-space distribution obtained from equation (15) with equations (13, 16, 8) is plotted in Figure 5. The distribution of high-amplitude motion in domain 2 has a moon shape. For small f, domain 2 becomes a ring, and the population is squeezed in amplitude. In region 1, the distribution is approximately Gaussian.

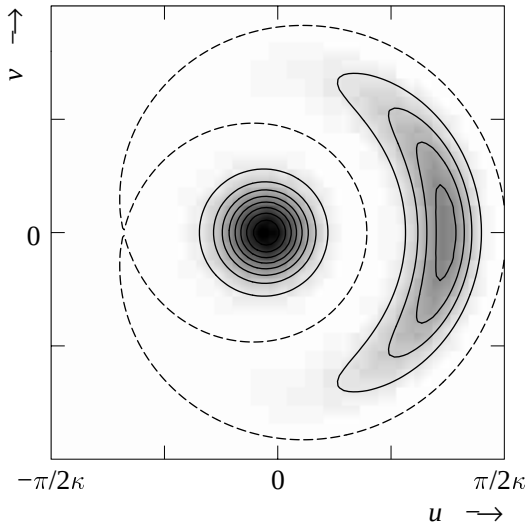

Fig. 5. Density plot of the stationary distribution $P(u,v)$. The same Hamiltonian as in Figure 4 is used. The temperature is taken $k_\mathrm{B}T=0.01m(\omega_0/\kappa)^2$. Some contour lines of constant density are shown. These coincide with the Hamiltonian orbits. Population density is zero on the instable orbit (dotted line).

6 Application I: Emission spectrum in transient spectroscopy

6.1 Free motion after switch-off

As long as the system is driven by the probe beam, all the excited trajectories have frequency δ. Consider for instance an atom located in the jth potential well with a motion

$$x_j(t)=a_j+\sqrt{2n}\,\cos(\phi+\delta t+j\pi-ka_j).$$

Note that the phase offset $(\kappa-k)a_j=j\pi-ka_j$ is determined by the phases of the lattice and of the probe beams at the potential minimum, so that the atomic distributions in all the wells will be determined by the same function $P(n,\phi)$. The light scattered by the atom has components of frequency ck, $ck\pm\delta$, ..., etc. Components that characterize the amplitudes of the bistable states can also be found but they occur because of the transient response associated with a spontaneous scattering event. They are thus much weaker, as can be inferred from the small value

of the ratio between the inelastic and elastic scattering components in an optical lattice [1,33].

Another method that has been used experimentally [9,34,35] is to switch abruptly the probe beam frequency to a new value ck' for which the atoms are transparent. The atomic orbits become free, with amplitude n', phase ϕ' and frequency $\omega(n')$. In the rotating-wave approximation, the trajectories of atoms in potential well j after the switch-off are

$$x'_j(t) = a_j + \sqrt{2n'}\,\cos(\phi' + \omega(n')t + j\pi - ka_j) \qquad (17)$$

on the time scale where dissipation is not yet effective. The excited trajectories now have a spectrum of vibrational frequencies.

During the sudden switch-off, position and momentum do not change. Hence, the relationship between the new values n', ϕ' and the old values n, ϕ follows from continuity in position and momentum x and p. If the atoms are released at $t = 0$, the amplitude and phase of the driven and free motion are related by $\sqrt{n'/n} = \cos\phi\,/\cos\phi' = \delta\sin\phi\,/\omega(n')\sin\phi'$. This gives $n' \approx n$ and $\phi' \approx \phi$ if δ is in the vicinity of $\omega(n')$. More precisely, the values before switch-off can be explicitly expressed as functions $n(n', \phi')$ and $\phi(n', \phi')$ of the values after the switch-off by

$$\begin{aligned} n &= n'\cos^2\phi' + \frac{\omega^2(n')}{\delta^2}n'\sin^2\phi', \\ \phi &= \arctan\frac{\omega(n')\tan\phi'}{\delta}\,\cdot \end{aligned} \qquad (18)$$

This determines the distribution P' of the amplitude and phase after the probe cut-off in terms of the original distribution P. By looking at the density in phase space one obtains

$$P'(n', \phi') = P(n, \phi)\sqrt{\frac{\omega(n')}{\delta} - \frac{K(n')}{\delta\omega(n')}\sin^2\phi'}.$$

Here, the explicit solutions (18) must be substituted. The Jacobian can be most easily obtained *via* the ordinary position and momentum variables. The mechanical energy of an atom before and after the switch-off is

$$\begin{aligned} E &= \frac{m}{2}\Big[\delta^2 n + U(n) + (\delta^2 - \omega^2(n))n\cos 2\phi\Big], \\ E' &= \frac{m}{2}\Big[\omega^2(n')n' + U(n')\Big]. \end{aligned}$$

Since position and momentum do not change if the switching time is fast, the mechanical energy is conserved. Hence the amplitude n' can also be determined from $E'(n') = E(n, \phi)$.

6.2 Emission signal

We consider the transient photon emission just after the switch-off, but well before the atoms have relaxed into their ground state again. These photons are scattered from the carrier waves of the optical lattice. Because the probe beam has forced a phase relation between the vibrational motion of the atoms in the different wells, the scattered field is predominantly in the same angular direction as the probe beam, the x-direction. The field emitted in this direction is

$$\mathcal{E}(t) \sim \mathrm{e}^{-\mathrm{i}kct}\int \mathrm{d}n\mathrm{d}\phi\, P'(n, \phi) \times \sum_j \Big[\mathrm{e}^{-\mathrm{i}(k+\kappa)x'_j(t)}\eta_+ + \mathrm{e}^{-\mathrm{i}(k-\kappa)x'_j(t)}\eta_-\Big].$$

The atomic coordinates, $x'_j(t)$, given by equation (17) for an atom in well j, with initial amplitude n and phase ϕ determine the phases of the scattered waves. The summation runs over the potential wells j. The two exponents describe the emission of a photon in the x-direction, which follows the absorption of a photon from one of the lattice waves. The relative strengths η_+ and η_- of the contribution of the two opposite directions depend on the specific atomic transition and the polarization of the lattice waves. The calculation of the numerical prefactors $\eta_\pm$ involve the same parameters as the prefactors $\varepsilon_\pm$ in the expression (1) of the optical potential. In some cases, it can be shown that they are proportional (for instance in the $1/2 \to 3/2$ transition and jumping regime). Because the trajectories of different atoms evolve at a different frequency, there is a washout in the interference of the emitted field in the x-direction, and the amplitude decays.

For $t > 0$, the beat signal along the probe axis normalized to one atom is

$$\tilde{S}(t) = \int \mathrm{d}n\mathrm{d}\phi\, P'(n, \phi)g(n)\cos(\phi + \omega(n)t + ckt - ck't),$$

with

$$g(n) = \eta_+ J_1((k+\kappa)\sqrt{2n}) + \eta_- J_1((k-\kappa)\sqrt{2n}).$$

Here the Bessel functions J_1 arise from the interference of the contributions from the different wells. The signal has the Fourier transform $S(\Omega)$. By denoting $\omega = \Omega - ck + ck'$,

$$S(\omega) = \frac{\mathrm{i}}{2}\int \mathrm{d}n\,\frac{g(n)}{\omega - \omega(n) + \mathrm{i}0_+}\int \mathrm{d}\phi\, P'(n, \phi)\mathrm{e}^{-\mathrm{i}\phi}. \qquad (19)$$

In the low-friction limit, the factor $\mathrm{e}^{-\mathrm{i}\phi}$ in the integral can be replaced by $\cos\phi$, because P is then an even function of ϕ. When the spectra are examined, two peaks can be resolved for sufficiently low temperatures or force. The peaks are located at $\omega \approx \omega_2 \approx \delta$ and $\omega \approx \omega_1 \approx \omega_0$. For moderate values of the force f, the two peaks in the distribution $P(n, \phi)$ are of comparable width, so that the spectral peak around ω_2 is broader, since there the frequencies have a wider range. For small f, the peak around ω_2 becomes narrower, due to the squeezing in phase space. A few calculated spectra are plotted in Figure 6.

7 Application II: Absorption spectrum

Although our calculation of the equilibrium distribution is based on the zero-friction limit, we can still use the

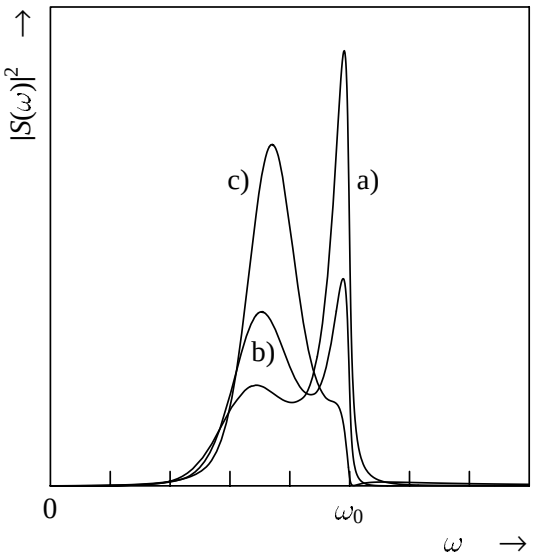

Fig. 6. Transient emission spectrum $|S(\omega)|^2$. The three curves correspond to the different detunings: (a) $\delta = 0.65\omega_0$, (b) $0.70\omega_0$, (c) $0.75\omega_0$. Force and temperature are $\kappa f = 0.015\omega_0^2$ and $k_{\rm B}T = 0.01m(\omega_0/\kappa)^2$ and we used the lattice parameters $\kappa = k/\sqrt{3}$, $\eta_1 = \eta_2$.

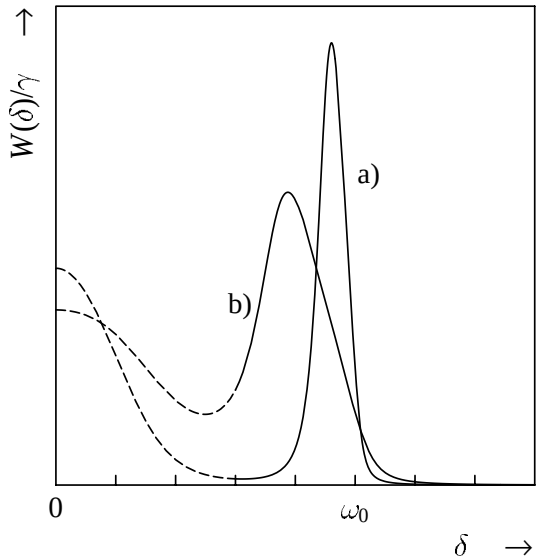

Fig. 7. Absorption spectra $W(\delta)$ in the low-friction limit. Values for the force are (a) $\kappa f = 0.005\omega_0^2$, (b) $\kappa f = 0.02\omega_0^2$, and the temperature is $k_{\rm B}T = 0.01m(\omega_0/\kappa)^2$. The same lattice parameters are used as in Figure 6. The weak peaks at $\delta = 0$ (dotted) are predicted mathematically for low values of the friction constant γ. They appear in the range where the rotating-wave approximation is invalid, and should not be considered as physical.

results to evaluate the absorption. This quantity can for instance be deduced from the work of the probe electric field [33]. A straight-forward calculation gives the steady-state absorption

$$W(\delta) = \int \mathrm{d}n\mathrm{d}\phi\, P(n,\phi) g(n) \sin\phi$$

in terms of the equilibrium distribution $P(n,\phi)$. In the case of zero friction, the distribution is of the form (15) and the absorption vanishes, because $P(n,\phi) = P(n,-\phi)$. However, we can use as a first approximation the distributions (11) with the populations α_1 and α_2 predicted by equations (14) of the zeroth order analysis. In the limit of low temperature, where narrow distributions in phase space are found, one can approximate for each component of the distribution the average of $g(n)\sin\phi$ by its value for the stationary solution. Using the relation $\sin\phi_i = \gamma\delta\cos\phi_i\,/(\delta^2 - \omega_i^2)$, one obtains to first order

$$W(\delta) = \frac{g(n_1)\gamma\delta}{\omega_1^2 - \delta^2}\alpha_1 + \frac{g(n_2)\gamma\delta}{\delta^2 - \omega_2^2}\alpha_2.$$

The high-amplitude motion gives rise to strong absorption. Outside the bistability interval, there exist only one stable state, and only a single term contributes. There absorption is weak. Examples of this absorption spectrum are plotted in Figure 7. In the low-friction approximation, we find that the high-amplitude mode is also excited near $\delta = 0$. This can only occur because for small γ the bistability interval extends all the way to $\delta_- = 0$ (see Fig. 2). In this region, however, the rotating-wave approximation is not reliable. The absorption spectrum thus gives less insight in the bistable dynamics than the emission spectrum.

As a final remark, we note that in the low-temperature approximation, the surprising relation $W(\delta) \sim \gamma S(\delta)$ between absorption and emission of the probe frequency is valid for $k' = k$, $n_i' = n_i$.

8 Summary and discussion

We have presented a study of the driven motion in an anharmonic potential well, under the action of fluctuations. This simple system is intended to model the recently observed splitting in the emission spectrum of an optical lattice driven by a weak probe beam [9,34]. Actually, the experimental spectra are similar to the curves shown in Figure 6 although the peaks look sometimes sharper.

The present model provides a reasonable qualitative understanding of the physics that occurs in a driven optical lattice. There remain, however, a few difficulties that prevent a full quantitative comparison with experiments. First, the friction and fluctuations must be added to the optical potential whilst in a real lattice it is the same field that provides the potential and the cooling. In the model presented here and contrary to the experimental case, it is possible to tune independently the potential and the temperature. In the plots shown in our letter [9], we have taken values of T compatible with the values predicted by the Sisyphus theory [13] for the optical potential V_1. However, a better agreement with the experimental curves can be found by tuning T independently of V_1. The curves presented in this paper, for example, have low temperatures but better fit the experimental data. A second drawback comes from the fact that friction and diffusion were assumed to be position independent. A third problem arises

with the one-dimensional approximation. Experiments are usually done in $3D$ lattices. Even if the probe beam excites the motion along an eigenmode of the linearized problem, nonlinear couplings between the various directions remain possible. However it is probably reasonable to neglect these couplings when the eigenvalues of the linearized problem are significantly different.

We think that most of these problems can be overcome by a numerical solution of the Fokker-Plank equation in a realistic bipotential [18,33], an approach which permits to treat in a self-consistent way the cooling and the potential. A first step in that direction was recently undertaken in collaboration with Peter Horak and provided phase-space distributions in qualitative agreement with those presented here.

The authors would like to thank P. Horak and A. Picon for helpful discussions. This work was supported by the European Commission (TMR network "Quantum Structures", contract FRMX-CT96-0077).

Appendix A: Damped motion

In this appendix we study the behaviour near the stationary points, when friction is included. Consider the low-amplitude stable point (u_1, v_1), near the maximum of the Hamiltonian. In order to evaluate the dynamics near this stable point in presence of friction, we expand the Hamiltonian. The rotated coordinates

$$\tilde{u} = \frac{(u-u_1)u_1 + (v-v_1)v_1}{\sqrt{2n_1}},$$
$$\tilde{v} = \frac{(v-v_1)u_1 - (u-u_1)v_1}{\sqrt{2n_1}}$$

are governed by the equations

$$\dot{\tilde{u}} = \frac{\mathrm{d}H_1}{\mathrm{d}\tilde{v}} - \frac{\gamma\tilde{u}}{2}, \quad \dot{\tilde{v}} = -\frac{\mathrm{d}H_1}{\mathrm{d}\tilde{u}} - \frac{\gamma\tilde{v}}{2}, \quad \text{with}$$
$$H_1(\tilde{u},\tilde{v}) = H(u,v) - \frac{\gamma\tilde{v}}{2}\sqrt{2n_1}. \tag{A.1}$$

Only in absence of friction, the new Hamiltonian $H_1(\tilde{u},\tilde{v})$ coincides with the original (symmetric) Hamiltonian $H(u,v)$ expressed in the new coordinates. Clearly, the damping drives the system to the stable solutions. To second order in $\tilde{u}$ and $\tilde{v}$, $H_1 = \varepsilon_1 + (\tilde{u}^2 c_1 + \tilde{v}^2 d_1)/2$. For the other stable state, of course, a Hamiltonian H_2 can be defined, so that similar equations hold for variables defined near (u_2, v_2). If the n-dependency of f is neglected, the coefficients in these Hamiltonians are

$$c_i = K(n_i)/\delta + d_i, \quad d_i = f u_i/2\delta n_i. \tag{A.2}$$

We note that $c_i + d_i = C_i$ as given by equation (12). The trajectories are spiralling inwards into the stable points (see Fig. 4)

$$\tilde{u}(t) = \pm\sqrt{a/c_1}\,\mathrm{e}^{-\gamma t/2}\sin 2\pi t/T_i,$$
$$\tilde{v}(t) = \sqrt{a/d_1}\,\mathrm{e}^{-\gamma t/2}\cos 2\pi t/T_i.$$

The amplitude is decreasing with time but the periods given by $T_i = 2\pi/\sqrt{c_i d_i}$ are constant. For small f, the frequencies of circulation about the stable points are given by

$$\frac{2\pi}{T_1(\varepsilon_1)} = \frac{1}{2\delta}(\omega_1^2 - \delta^2),$$
$$\frac{2\pi}{T_2(\varepsilon_2)} = \frac{\omega_0}{2\delta}\sqrt{(\delta^2-\omega_2^2)J_2(\kappa\sqrt{8n_2})}.$$

The oscillating motion in the ordinary position variable is thus modulated with these frequencies. For the low amplitude motion, the equation which is still correct if there is just one solution, can be recognized as the beat between a free solution (which is damped for non-zero γ) and the forced solution at the stationary point, just as for a driven harmonic oscillator. The oscillation frequency of the high amplitude solution is much larger than expected due to the nonlinearity of the potential. When we take the limit of zero friction, the Hamiltonians H_i and H become identical. The trajectories near the stable points become closed elliptical orbits with a constant energy ε and amplitudes determined by $a = 2(\varepsilon - \varepsilon_i)$.

Let us now consider the instable state. As ε increases and passes the critical energy ε_0, the orbits in domain 2 split into two parts at the saddle point (u_0, v_0), and go over into the two orbits of 1 and 3. In the vicinity of the saddle point, the trajectories are hyperboloids. On approaching the saddle point the two orbits slow down so that their orbit times diverge as

$$T_1(\varepsilon) = T_3(\varepsilon) = \frac{1}{2}T_2(\varepsilon) = \frac{1}{\sqrt{c_0 d_0}}\log\frac{n_0 d_0}{|\varepsilon - \varepsilon_0|}, \quad \varepsilon \downarrow\uparrow \varepsilon_0. \tag{A.3}$$

Close to the critical point, the motion in domains 1 and 3 for $\gamma = 0$ is symmetrical with respect to the vertical axis through the critical point.

Appendix B: Solving the Fokker-Planck equation in the low-friction limit

In this appendix the method used to derive the equilibrium distribution of the energy ε as given by the expression (13) is described. When the damping rate is small, motion on the fast time scale is almost Hamiltonian, and energy is well defined. As a lowest order solution one takes a pure (closed) Hamiltonian orbit. Then calculate the small energy change $\Delta\varepsilon$ along this orbit. One has to expand to second order in Δn and $\Delta\phi$ to include the effect of the noise, which is described by Ito calculus. Of course only the dissipative terms in equation (7) contribute. The secular approximation thus reduces the dynamical behavior to a single variable, the energy ε. On the slow time scale of the dissipation, the energy evolves according to the Langevin equation

$$\dot{\varepsilon} = -A(\varepsilon) + \sqrt{2B(\varepsilon)}\,\zeta(t). \tag{B.1}$$

This stochastic equation has noise source ζ, with $\langle\zeta(t')\zeta(t)\rangle = \delta(t'-t)$. For the moment we have neglected

that there can be two orbits for one energy value, and avoid the saddle point. In the Ito calculus, the drift and diffusion coefficients A and B are given by [31]

$$-AT = \overline{\langle \Delta\varepsilon \rangle}, \quad BT = \frac{1}{2}\overline{\langle (\Delta\varepsilon)^2 \rangle}.$$

There are two averages. We must integrate over one orbit time T but also take the average over all possible noise functions ξ, ξ'. In deriving these coefficients is consistent to lowest order to approximate $\mathrm{d}H/\mathrm{d}\phi = \dot{n}$, $\mathrm{d}H/\mathrm{d}n = -\dot{\phi}$ in the Taylor expansion of $\Delta\varepsilon$ in Δn and $\Delta\phi$. The result is

$$A = A' - \frac{\mathrm{d}}{\mathrm{d}\varepsilon}B, \quad A' = -\gamma\,\overline{n\dot{\phi}}, \quad B = D\,\overline{2n\dot{\phi}^2 + \dot{n}^2/2n}. \tag{B.2}$$

These coefficients are uniquely determined by the energy ε and the phase-space domain 1, 2 or 3. Note that we found that the contribution proportional to D in the drift rate A can be written as the derivative of the energy diffusion coefficient B. This will be of use later. The stochastic equation of motion (B.1) is equivalent to the Fokker-Planck equation for the time-dependent energy distribution $F_i(\varepsilon, t)$

$$\dot{F}_i = \frac{\mathrm{d}}{\mathrm{d}\varepsilon}\Big[A_i F_i + \frac{\mathrm{d}}{\mathrm{d}\varepsilon}B_i F_i\Big]. \tag{B.3}$$

We now include the full phase space so that we need the index i to denote the energy branches that correspond to the three domains in phase space. Conservation of the probability current implies that the term in brackets in equation (B.3) must vanishes at the end points ε_2 and ε_1. This is automatically the case, since at these points both $A' = 0$ and $B = 0$. This is, however, also the case at ε_0. This means physically that flow across the critical orbits occurs on an even slower timescale than the friction rate.

Although the energy $\varepsilon = H(n, \phi)$ of a particle is given by its coordinates, it does not determine the coordinates. In the secular approximation, a single particle contributes a periodic orbit to the total phase-space distribution. It follows from Hamilton's equations that this contribution equals

$$\int_0^T \mathrm{d}t\, \delta(n - n_i(\varepsilon, t))\delta(\phi - \phi_i(\varepsilon, t)) = \delta(\varepsilon - H(n, \phi)),$$

inside domain i. The time-dependent distributions $P(n, \phi, t)$ and $F_i(\varepsilon, t)$ are therefore related by expression (15). A similar relation for the energy distribution, was used in reference [29]. Here the distribution was first expressed in terms of the energy and velocity variables, after which the (fast) velocity variable was eliminated.

Fokker-Planck equation (B.3) is one dimensional and has a simple analytical steady-state solution

$$F_i(\varepsilon) = F_i(\varepsilon_0) \exp -\int_{\varepsilon_0}^{\varepsilon} \mathrm{d}\varepsilon'\, \frac{A_i'(\varepsilon')}{B_i(\varepsilon')} \tag{B.4}$$

on each of the three energy branches. Note that this solution is expressed in terms of the simpler coefficient A' defined in equation (B.2) instead of the original coefficient A of equation (B.3). Since the flow rate across the critical orbit is much slower than γ, the populations of the three domains only becomes balanced when the distributions inside are already in equilibrium. Therefore, a hysteresis cycle can in principle be observed, provided that the parameters are varied adiabatically, but not slower that this weak thermalisation rate.

The drift and diffusion coefficients $A_i'(\varepsilon)$ and $B_i(\varepsilon)$ can be expressed as integrals over n only, after ϕ is eliminated with Hamilton's equations. Substituting these in equation (B.2) gives

$$A_i'(\varepsilon)T_i(\varepsilon) = 2\gamma \int \mathrm{d}n\, \frac{2\delta\varepsilon + U + \delta^2 n - 2\omega^2 n}{\sqrt{8f^2 n - (2\delta\varepsilon + U - \delta^2 n)^2}},$$

$$B_i(\varepsilon)T_i(\varepsilon) = \frac{2D}{\delta} \int \mathrm{d}n\, \frac{f^2 + 2(\delta^2 - \omega^2)(2\delta\varepsilon + U - \omega^2 n)}{\sqrt{8f^2 n - (2\delta\varepsilon + U - \delta^2 n)^2}},$$

and the periods are given by equation (16). The integration intervals range from the minimum to the maximum value of n on the orbit. Although, the friction and diffusion coefficients A' and B become zero at the critical orbits, the time integrated coefficients $A'T$ and BT are nonzero. This means that the gradients of F_i are finite at the boundaries. It follows from (A.3) that this weak flow across the borders only occurs near the saddle point where the orbits slow down. It is therefore possible to make the energy distribution continuous at ε_0, provided that one compares to sum $F_1(\varepsilon) + F_3(\varepsilon)$ above ε_0 with $F_2(\varepsilon)$ below ε_0. That this is reasonable can be seen by examining the behaviour at the borders of the three phase space domains (see Fig. 4). Because the orbits of 2 split up in two contributions in 1 and 2, the drift and diffusion coefficients divide up in the same way. The symmetry between the domains 1 and 3 gives that

$$F_1(\varepsilon_0) = F_3(\varepsilon_0) = F_2(\varepsilon_0)/2. \tag{B.5}$$

This balance serves as a boundary condition to determine the full equilibrium solution (B.4).

It turns out that the behavior of $A'T$ and BT is almost linear over the full energy range. This results in the approximate expressions

$$A_i'(\varepsilon)T_i(\varepsilon) = (\varepsilon - \varepsilon_i)\gamma T_i(\varepsilon_i),$$
$$B_i(\varepsilon)T_i(\varepsilon) = |\varepsilon - \varepsilon_i| D C_i T_i(\varepsilon_i),$$

for $i = 1, 2$, with C_i defined in equation (12). In addition,

$$A_3'(\varepsilon)T_3(\varepsilon) = A_2'(\varepsilon)T_2(\varepsilon) - A_1'(\varepsilon_0)T_1(\varepsilon_0),$$
$$B_3(\varepsilon)T_3(\varepsilon) = B_2(\varepsilon)T_2(\varepsilon) - B_1(\varepsilon_0)T_1(\varepsilon_0),$$

so that friction and diffusion are continuous across the critical orbit. Substitution of these approximations in the formal solution equations (B.4, B.5) results in the expressions (13).

The consistency with expression (11) in the regime of low temperature can now be verified. When the solution for F_i is substituted in equation (15), one obtains

equation (11), provided T_i is take as a constant. This can be seen as a good approximation in the neighbourhood of the stable points. One also finds the same values for the populations α_i, when taken at low temperature.

References

1. P.S. Jessen, I.H. Deutsch, in *Advances in Atomic, Molecular and Optical Physics*, edited by B. Bederson, H. Walther (Academic Press, 1996), Vol. 37, p. 95.
2. G. Grynberg, C. Triché, in Coherent and collective interactions of particles and radiation beams, *Proceedings of the International School of Physics Enrico Fermi*, Course CXXXI (IOS, Amsterdam, 1996), pp. 243-287.
3. A. Hemmerich, M. Weidenmüller, T.W. Hänsch, in Coherent and collective interactions of particles and radiation beams, *Proceedings of the International School of Physics Enrico Fermi Course CXXXI* (IOS, Amsterdam, 1996) pp. 503-528.
4. D.R. Meacher, Contemp. Phys. **39**, 329 (1998).
5. G. Raithel, W.D. Philips, S. Rolston, Phys. Rev. Lett. **81**, 3615 (1998).
6. O. Morsch, P.J. Jones, D.R. Meacher, Phys. Rev. A **61**, 023410 (2000).
7. P. Verkerk, B. Lounis, C. Salomon, C. Cohen Tannoudji, J.Y. Courtois, G. Grynberg, Phys. Rev. Lett. **68**, 3861 (1992).
8. M.G. Raizen in *Advances in Atomic, Molecular and Optical Physics*, edited by B. Bederson, H. Walther (Academic Press, 1999), Vol. 41, p. 43.
9. G. Grynberg, C. Triché, L. Guidoni, P.M. Visser, Europhys. Lett. **51**, 506 (2000).
10. L.D. Landau, E.M. Lifshitz, *Mechanics* (Pergamon Press, Oxford, 1960).
11. A.E. Kaplan, Phys. Rev. Lett. **48**, 138 (1982); Phys. Rev. Lett. **56**, 456 (1986).
12. G. Gabrielse, H. Dehmelt, Phys. Rev. Lett. **54**, 537 (1985).
13. C. Cohen-Tannoudji, in Fundamental Systems in Quantum Optics, *Les Houches Summer School*, Session LIII, edited by J. Dalibard, J.M. Raimond, J. Zinn-Justin (Elsevier, 1992).
14. L.A. Lugiato, *Progress in Optics*, edited by E. Wolf (North Holland, 1984), Vol. XXI.
15. D. Enzer, G. Gabrielse, Phys. Rev. Lett. **78**, 1211 (1997).
16. S. Habib, K. Shizume, W.H. Zurek, Phys. Rev. Lett. **80**, 4361 (1998).
17. W.T. Strunz, L. Diósi, N. Gisin, T. Yu, Phys. Rev. Lett. **83**, 4909 (1999).
18. K.I. Petsas, A.B. Coates, G. Grynberg, Phys. Rev. A **50**, 5173 (1994).
19. C. Cohen Tannoudji, J. Dupont-Roc, G. Grynberg, *Atom-Photon Interactions* (Wiley, New York, 1992).
20. J.D. Miller, R.A. Cline, D.J. Heinzen, Phys. Rev. A **47**, R4567 (1994).
21. S. Friebel, C. d'Andrea, J. Walz, M. Weitz, T.W. Hänsch, Phys. Rev. A **57**, R20 (1998).
22. D. Boiron, A. Michaud, J.M. Fournier, L. Simard, M. Sprenger, G. Grynberg, C. Salomon, Phys. Rev. A **57**, R4106 (1998).
23. G. Nienhuis, P. van der Straten, Phys. Rev. A **44**, 462 (1991).
24. Y. Castin, J. Dalibard, Europhys. Lett. **14**, 761 (1991).
25. K.J. Petsas, G. Grynberg, J.Y. Courtois, Eur. Phys. J. D **6**, 29 (1999).
26. Nobel Lectures: S. Chu, C. Cohen Tannoudji, W.D. Phillips, Rev. Mod. Phys. **70**, 685 (1998).
27. S. Neil Rasband, *Chaotic Dynamics of Nonlinear Systems* (John Wiley & Sons, New York, 1990).
28. J.M.T. Thompson, H.B. Stewart, *Nonlinear dynamics and chaos* (John Wiley & Sons, New York, 1986).
29. H. Risken, *The Fokker-Planck Equation* (Springer, New York, 1998).
30. P. Bergé, Y. Pomeau, C. Vidal, *Order within Chaos* (Wiley, 1986).
31. N.G. van Kampen, *Stochastic Processes in Physics and Chemistry* (North-Holland, 1981).
32. C.W. Gardiner, *Stochastic Methods for Physics, Chemistry and the Natural Sciences* (Springer-Verlag, Berlin, 1983).
33. J.Y. Courtois, G. Grynberg, Phys. Rev. A **46**, 7060 (1992).
34. C. Triché, Ph.D. thesis, École Polytechnique, Paris, 1997.
35. C. Triché, L. Guidoni, P. Verkerk, G. Grynberg, *OSA TOPS on Ultracold Atoms and BEC 1996*, edited by K. Burnett, Vol. 7, pp. 82-85, 1997.